



LAWRENCE
LIVERMORE
NATIONAL
LABORATORY

Model-Based Failure Detection for Cylindrical Shells from Noisy Vibration Measurements

J. V. Candy , B. L. Guidry, K. A. Fisher, D. H.
Chambers, E. Breidfeller

June 5, 2014

Journal of the Acoustical Society of America

Disclaimer

This document was prepared as an account of work sponsored by an agency of the United States government. Neither the United States government nor Lawrence Livermore National Security, LLC, nor any of their employees makes any warranty, expressed or implied, or assumes any legal liability or responsibility for the accuracy, completeness, or usefulness of any information, apparatus, product, or process disclosed, or represents that its use would not infringe privately owned rights. Reference herein to any specific commercial product, process, or service by trade name, trademark, manufacturer, or otherwise does not necessarily constitute or imply its endorsement, recommendation, or favoring by the United States government or Lawrence Livermore National Security, LLC. The views and opinions of authors expressed herein do not necessarily state or reflect those of the United States government or Lawrence Livermore National Security, LLC, and shall not be used for advertising or product endorsement purposes.

Model-based failure detection for cylindrical shells from noisy vibration measurements

J. V. Candy B. L. Guidry K. A. Fisher D. H. Chambers E. Breidfeller

University of California

Lawrence Livermore National Laboratory

P.O. Box 808, L-156

Livermore, CA 94551

Phone: 925-422-8675

Email: candy1@llnl.gov

Model-based processing is a theoretically sound methodology to address difficult objectives in complex physical problems involving multichannel sensor measurement systems. It involves the incorporation of analytical models of both physical phenomenology (complex vibrating structures, noisy operating environment, etc.) and the measurement processes (sensor networks and including noise) into the processor to extract the desired information. In this paper, a model-based methodology is developed to accomplish the combined task of on-line failure monitoring and classification for vibrating cylindrical shell externally excited by controlled vibrational excitations. A model-based processor is formulated to: (1) monitor system performance; (2) detect potential failure conditions; (3) isolate the failure mechanism using classifiers; and (4) determine the overall condition of the underlying system. The objective of this paper is to develop a real-time, model-based monitoring scheme for on-line diagnostics in a representative structural vibrational system.

PACS numbers: 43.60Gk, 43.30Zk

I. INTRODUCTION

Structural vibration systems¹ operating over long periods of time can be subjected to component and overall system failures due to fatigue caused by external excitations or by cracking and resonances during the aging process¹⁻⁶. In some cases the system can fail catastrophically, causing complete deterioration of the overall structure and the consequences that follow. It is essential to provide timely information about component failure and the conditions leading up to it, as well as prognosticating about the integrity of the total system in the future.

A model-based approach^{7–11} to develop diagnostic techniques for structural failure prediction is based on a well-established theoretical formalism that ensures a careful and systematic analysis of the vibrational system or classes of systems under investigation and their associated failure mechanisms. Models can be developed from a first-principles mathematical representation, or by utilizing sensor measurements to “fit” the model parameters to the data—the approach we pursue in this paper. In cases where the failure mechanism is not well understood, the model fitting approach offers an effective solution. In fact, in contrast to many approaches of solving this problem, this model-based approach does not require an explicit representation of the failure mechanism at all to design an on-line monitor for initial failure detection. It is based on obtaining a representation of the vibrating structure during normal certification operations, or even more desirable, during quality assurance or acceptance testing. Once these normal operational characteristics of the system are known, the processor is developed based on the properties of the so-called residuals or innovations sequence. This sequence is the difference between the measured and predicted sensor outputs obtained from the underlying normal structural system model. Once this condition or “difference” monitor detects a failure, it is then classified according to a set of well-established failure mechanisms.

Failure detection for mechanical systems has long been the subject of much research with most of the work being concentrated on single-channel, spectral or cepstral analysis techniques for diagnostic purposes.² There have been several successful applications of the model-based approach^{8–17} to these type problems, but none devoted to solving the complete failure condition detection, failure isolation, and time-to-failure prediction problem for a real-time maintenance problem. The inclusion of a process model in any signal processing scheme provides a means of introducing information in a self-consistent manner.^{18–21} This is shown in Fig. 1 where we observe how vibrational measurements are input to a model-based processor (*MBP*) utilized to provide information to the failure monitor.

As mentioned, structural vibration systems operating over long periods of time can be subjected to failures due to fatigue caused by various external forces or simply the aging process. When this happens it is possible for the structure to deteriorate causing a complete malfunction and possibly catastrophic failure. Thus, to attain reliable system performance it is

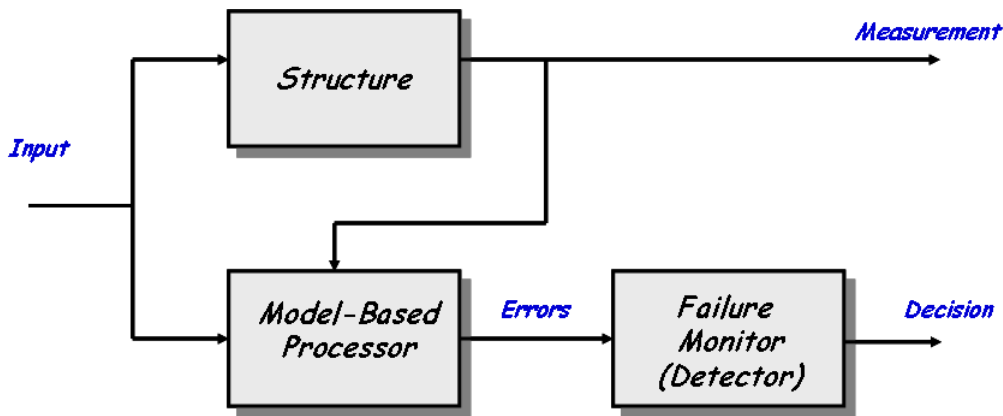


Figure 1: Conceptual model-based failure monitor.

necessary to monitor critical structural components, to provide timely information about current and/or imminent failures, and to predict its integrity. Standard approaches to detect failure mechanisms at the onset range from a simple accelerometer strategically placed, to observing the Fourier spectrum of known response, to using cepstral analysis to identify periodic responses, to sophisticated Bayesian processing schemes.^{22–27} Measures of failure can deteriorate significantly if noise is present - a common situation in an operational environment. A model-based signal processing approach⁸ to solve the structural system failure detection and classification problem is depicted in Fig. 2. Here we see that the first step is monitoring the current condition of the underlying structure. Should a failure be detected, a classifier processes the data to report the final condition and type of failure incurred.

Most of the current monitoring approaches for failure detection and isolation lead to single-channel processing of measured sensor data.¹ For instance, the so-called waterfall vibrational spectral plot, or the equivalent Campbell diagram³, is limited to a stacking display of single-channel spectral information to identify failures. Multiple sensors (such as accelerometers for vibrations, microphones for acoustics, and thermocouples for temperature) in a structure provide enhanced information about the system. This implies a multi-channel (multi-input, multi-output) system representation, which is most easily handled in state-space form¹, without restrictions to

¹The state-space representation of a system is the transformation of an n^{th} -order set of differential equations describing the system to a set of n first-order differential equations.

single-channel spectral representations. Once this is accomplished, then the process model of the structural system can be incorporated into an effective signal processing scheme. This representation leads to the model-based approach, which can be stated as “incorporating mathematical models of both physical phenomenology and the measurement processes including noise into the processor to extract the desired information.” The incorporation of a mathematical model that represents the phenomenology under investigation can vastly improve the performance of any processor, provided such model is accurate.^{8,17} We summarize the development and application of such on-line “model-based processors” (*MBP*) in the context of failure detection/isolation and failure prediction. The major advantages of model-based processors include are: recursive; statistical (incorporating both noise and parameter uncertainties); *not* constrained to stationary statistics; capable of being extended to incorporate both linear and nonlinear time-varying models; capable of on-line processing of the measured data at each iteration; capable of filtering the noisy measurements as well as simultaneously estimating the underlying states (vibrational responses, modes, etc.); capable of monitoring their own performance by testing the residual (or innovations) between the measurement and its prediction and easily extended to perform adaptively. However, a potential *drawback* is the increased computational load required that can be mitigated somewhat by the high speed/high throughput microprocessors currently available along with the possibility of parallel implementation.

As illustrated in Fig. 3 model-based signal processing involves incorporation of the process model (large-scale structure), measurement model (sensor network), and noise models (instrumentation, environmental, parameter uncertainty, etc.) along with measured data into a sophisticated processing algorithm capable of detecting, filtering (estimating), and isolating a mechanical failure in a hostile operational environment. This technique offers a well-founded statistical approach for comparing process/measurement/failure models to measured data and is not constrained to a stationary process, which is essential in the expected environment. A model-based processor provides estimates of various quantities of high interest (modes, vibrational response, resonances, etc.), and also provides on-line statistical performance measures which are especially useful for failure propagation experiments.

The model-based approach for failure detection, classification and predic-

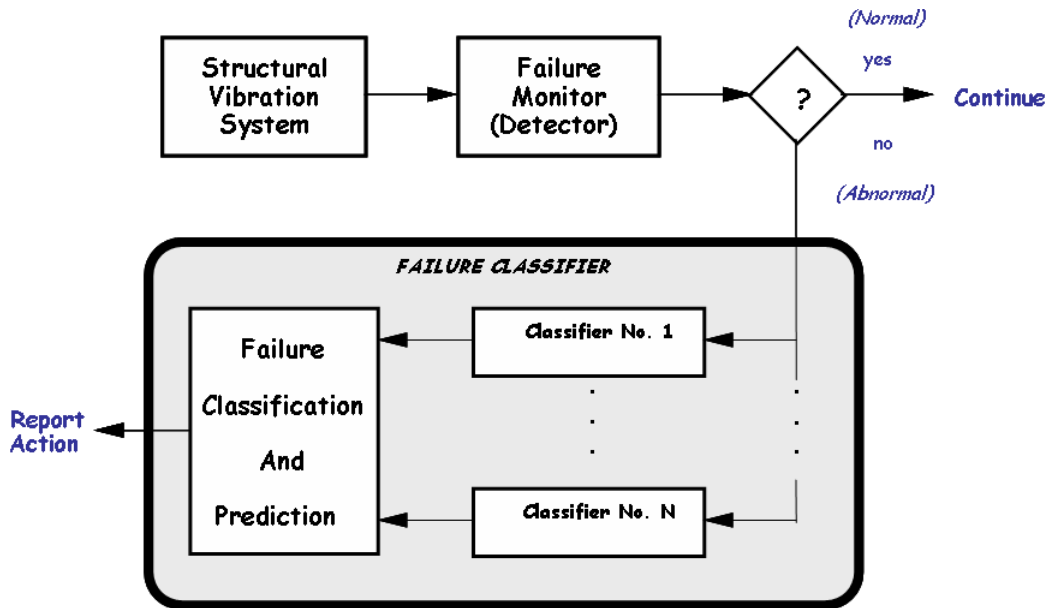


Figure 2: Model-based failure monitor and classifier structure.

tion (shown in Fig. 2) is based on the concept that the process or vibrational system under consideration is modeled either from first principles or using system identification techniques^{15,16,19} to “fit” models to the data. Once the system models are developed, then the sensor suite (or measurement system) models are developed. Usually the bandwidth of each sensor is much wider than the dominant dynamics or resonances of the system, and therefore each sensor is represented by a gain. However, if sensor dynamics must be included in the system model, the model-based approach easily accommodates them. Sensor dynamics models can be obtained from manufacturer specifications, independent experiments, or transfer function estimation to name a few (see section II some details). After these models are completed, then it remains to model the noise. If noise data are unavailable, then a reasonable approach is to model the noise as additive and random, leading to a Gauss-Markov model.¹⁹ Once a representation of the overall system (structure, sensors, and noise) is developed, then a failure monitor/detector can be developed to monitor the status of the vibrational system. Should a failure (that is, a deviation from the normal operation) be detected, then this failure must be classified using information from known or measured failures. Then

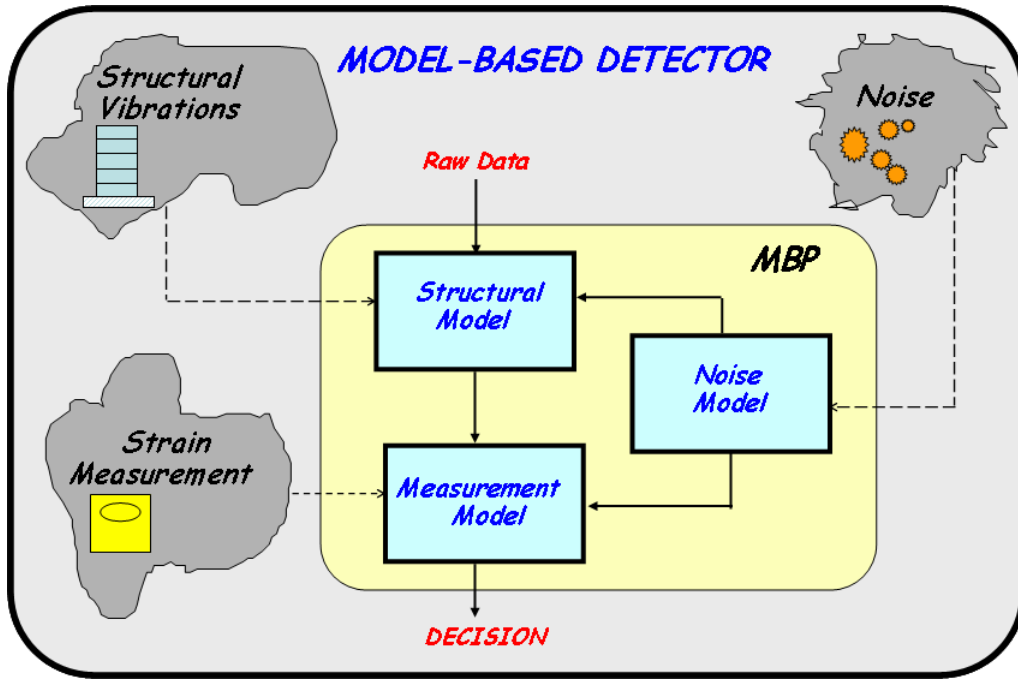


Figure 3: Model-based processor implementation incorporating process (cylinder), measurement (optical strain sensors) and noise (background, excitation) processes into a failure monitor/detector.

it is possible to predict the time-to-failure for the overall system, and decide on the appropriate action, including simply reporting the results.

In section II, we discuss the basic models of the cylinder system under investigation along with both distributed and lumped governing dynamic systems as well as the embedded novel optical strain measurement sensor employed. Next we present the fundamental model-based approach in section III including the underlying failure detection and classification problems. The model-based processor is developed in section IV and applied to simulated and experimental data in V. We summarize our results and discuss future work in the final section.

II. DYNAMIC MODELING OF A VIBRATING CYLINDER AND STRAIN SENSOR NETWORK

In this section we discuss the basic dynamic models used to represent the vibrating cylinder under study for failure detection along with the novel optical strain sensor network. We start with the fundamental wave dynamics and corresponding numerical model using a finite element approach. Next we discuss a coupled lumped multivariable dynamic model and corresponding transfer function matrices that provide the structure and justification of the *MBP* employed in the failure detector.

The fundamental governing equation for the vibrating elastic cylinder is⁵

$$\rho \frac{\partial^2 \mathbf{u}}{\partial t^2} - \mu \nabla^2 \mathbf{u} - (\lambda + \mu) \nabla (\nabla \cdot \mathbf{u}) = \rho \mathbf{f} , \quad (1)$$

where $\mathbf{u}(\mathbf{x}, t)$ is the vector displacement field, $\mathbf{f}(\mathbf{x}, t)$ is the forcing function, ρ is the material density, and λ and μ are the material elastic moduli.

This equation, along with the boundary conditions, describes the dynamic response of the cylinder to a given set of applied forces. We can convert this to a lumped model using a set of orthonormal vector basis functions $\mathbf{u}_n(\mathbf{x})$ such that

$$\int \mathbf{u}_m(\mathbf{x}) \cdot \mathbf{u}_n(\mathbf{x}) , d\mathbf{x} = \delta_{mn}$$

The displacement field and forcing excitation can be expanded in terms of these basis functions as:

$$\mathbf{u}(\mathbf{x}, t) = \sum_{n=1}^{N_d} d_n(t) \mathbf{u}_n(\mathbf{x}), \quad \mathbf{f}(\mathbf{x}, t) = \sum_{n=1}^{N_d} p_n(t) \mathbf{u}_n(\mathbf{x})$$

which leads to the following matrix equation for the coefficients $d_n(t)$:⁶

$$M\ddot{d}(t) + C\dot{d}(t) + Kd(t) = p(t) \quad (2)$$

where d is the $N_d \times 1$ displacement vector, p is the $N_p \times 1$ excitation force, and M , C , K , are the $N_d \times N_d$ lumped mass, damping function, and spring constant matrices characterizing the structural process model, respectively.

$$M = \begin{bmatrix} M_1 & 0 & 0 & 0 & 0 \\ 0 & M_2 & 0 & 0 & 0 \\ \vdots & \vdots & \ddots & \vdots & \vdots \\ 0 & 0 & 0 & M_{N_d-1} & 0 \\ 0 & 0 & 0 & 0 & M_{N_d} \end{bmatrix}, \quad C = [c_{ij}], \quad \text{and}$$

$$K = \begin{bmatrix} (K_1 + K_2) & -K_2 & 0 & 0 & 0 \\ -K_2 & (K_2 + K_3) & \ddots & 0 & 0 \\ 0 & \ddots & \ddots & -K_{N_d-1} & 0 \\ 0 & 0 & -K_{N_d-1} & (K_{N_d-1} + K_{N_d}) & -K_{N_d} \\ 0 & 0 & 0 & -K_{N_d} & K_{N_d} \end{bmatrix}$$

Though the damping function is not explicitly part of the original governing equation, it is standard practice to include damping in the lumped model. This model is in the form of a linear dynamical system, which can be converted to a state-space representation for signal processing purposes.

That is, if we define the $2N_d$ -state vector as $x(t) := \begin{bmatrix} d(t) & \dot{d}(t) \end{bmatrix}$, then the state-space representation of this process can be expressed as

$$\begin{aligned} \dot{x}(t) &= Ax(t) + Bu(t) \\ \dot{x}(t) &= \left[\begin{array}{c|c} 0 & I \\ \hline M^{-1}K & M^{-1}C \end{array} \right] x(t) + \left[\begin{array}{c} 0 \\ \hline M^{-1} \end{array} \right] p(t) \\ &\text{and} \\ y(t) &= \left[M^{-1} \mid 0 \right] x(t) \end{aligned} \tag{3}$$

where we have assumed that a sensor directly proportional to displacement is used, $y \in \mathcal{R}^{N_d \times 1}$.

For our measurement system we actually use a *Bragg fiber optic* strain sensor that is small ($< 1\text{mm}$ diameter), can use multi-wavelengths for multiple sensing points (multichannel receiving string or array) and is driven by

a tunable external laser source. Fiber Bragg grating (*FBG*) sensors measure changes in the light reflected and transmitted through a grating imprinted in the fiber as shown in Fig. 4a. Here light from the external laser source incident on the fiber Bragg grating is reflected and transmitted through the grating providing a measurement that is directly proportional to the strain induced by an impact device exciting the cylindrical shell and measured by a sensor network (as seen in Fig. 4b,c) and digitized for model-based processing.

The experimental system is comprised of a horizontally orientated aluminum cylinder (297mm long, and 196mm in diameter with a wall thickness of 2mm), supported above the optical bench by thin nylon lines. Actuation of the cylinder (input signal) was accomplished by a thin 080in diameter threaded rod, bolted to the cylinder surface and driven by an electro-dynamic shaker. The actuator is connected to an arbitrary waveform generator, allowing for precise control and tailoring of the input signal during the experiment. The inertial effects on the cylinder from the shaker, are minimized by mounting the shaker independently, on a separate external support. These efforts were motivated by a desire to generate a point source normal to the surface of the cylinder, and minimize complicated edge effects. Essentially, the cylinder is freely supported in space and driven by a point source normal to the surface. The cylinder has several locations where a concentrated mass can be attached to the surface. This facilitates a simple method to introduce a *known* change the system response with minimal error.

The response of the system from the point force is monitored using fiber Bragg sensors bonded to the outer surface of the cylinder. The physical principle behind the *FBG* sensor is that a change in strain, stress, or temperature will alter the center of the wavelength of the light reflected from an *FBG*. The power (reflected or transmitted) is directly proportional to the strain (displacements) in the fiber and the structure. Thus, *FBGs* offer a passive, minimally-invasive technique to monitor the structural response of the experimental cylinder assembly.

The size and mass of the sensors (dia < 0.5mm and mass/unit length << 0.1gm/cm) mitigates any loading effects that the sensors could introduce on the dynamic response of the cylinder. The spatial extent of the sensing region of the fiber Bragg sensor (including glue patch) on the surface of the cylinder is approximately 0.5cm². Two sensors were attached to the surface of the

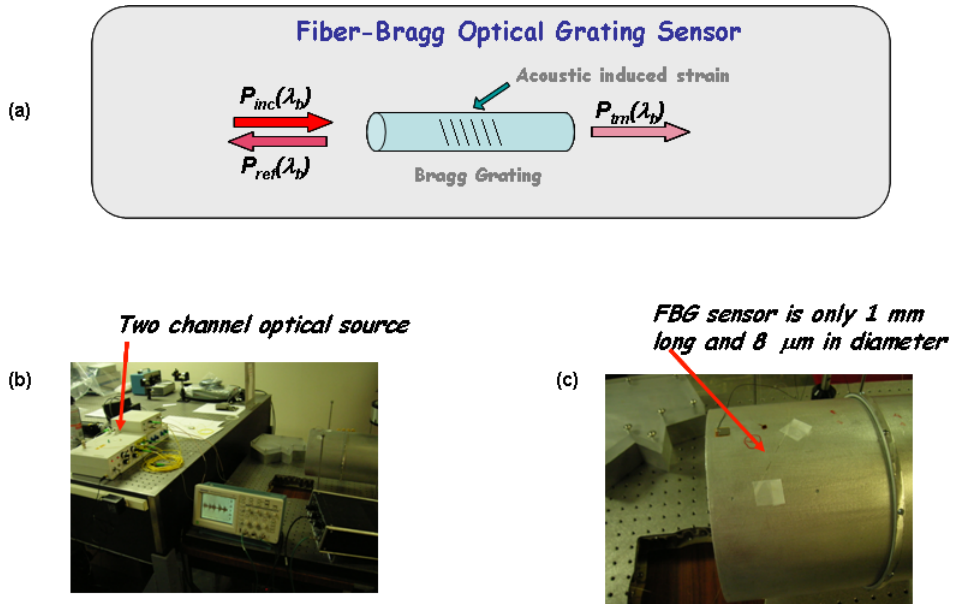


Figure 4: Fiber-Bragg optical strain sensor and hardware: (a) Optical sensor. (b) Experimental hardware set-up for vibrational excited cylinder strain measurements. (c) Sensor locations on cylinder.

cylinder, one at the horizontal center and the other, at the far end of the cylinder off axis.

The corresponding vector measurement is given by

$$y(t) = Cx(t) \quad (4)$$

A. Fiber Bragg Sensors^{28–31}

The physical principle (Fig. 5) behind the *FBG* sensor is that a change in strain, stress, or temperature will alter the center of the wavelength of the light reflected from an *FBG*. The *FBG* wavelength filter consists of a series of perturbations in the index of refraction along the length of the doped optical fiber. This index grating reflects a narrow spectrum of light that is directly proportional to the period of the index modulation (grating) in the fiber core. As the fiber is strained the period of the grating is altered, resulting in a modulation of the optical power that is reflected and transmitted. The modulation of the optical power is measured as AC voltage on a photodiode. Since a *FBG* sensor is typically bonded to an elastic structure, any change in

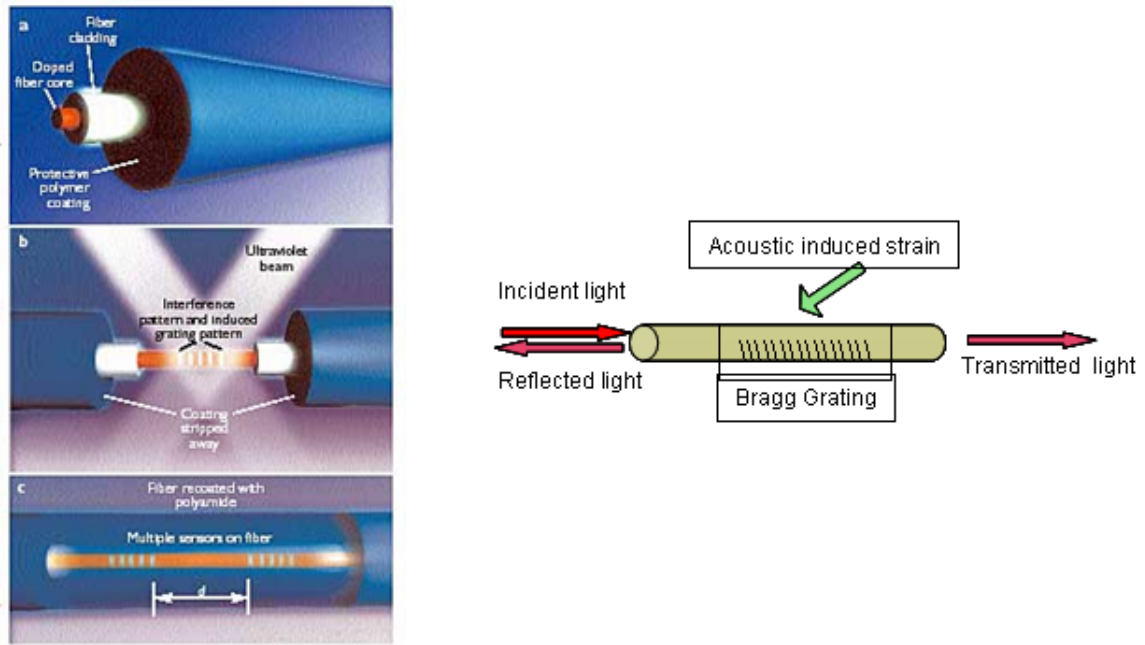


Figure 5: Multiple *FBG* sensors can be imprinted into the inner core of a fiber through the use of interfering ultraviolet beams. The interference patterns are essentially “burned” into the fiber core. The reflectivity of these grating regions is sensitive to a specific wavelength λ_n . Thus each sensor can be interrogated using a different wavelength from a tunable laser and using wavelength division multiplexing technology.

strain in the underlying structure is directly transmitted into the fiber. *FBG* sensors are routinely used to monitor dynamic vibrations in a wide variety of elastic structures.

The system scan frequency is a combination of the speed of the optical source, the bandwidth of the detectors, the data acquisition rate, and the rate at which the analysis of the wavelength shift can be performed. External cavity diode lasers (ECDLs) provide even higher output power than fiber lasers, which increases the number of sensors and the dynamic range. The narrow line-widths, fast sweep speeds, higher output power, and high side-mode suppression ratios of ECDLs improve the accuracy and dynamic range of *FBG* sensor systems. Moreover, incorporating a swept-wavelength meter improves system accuracy. Although the laser-based *FBG* systems

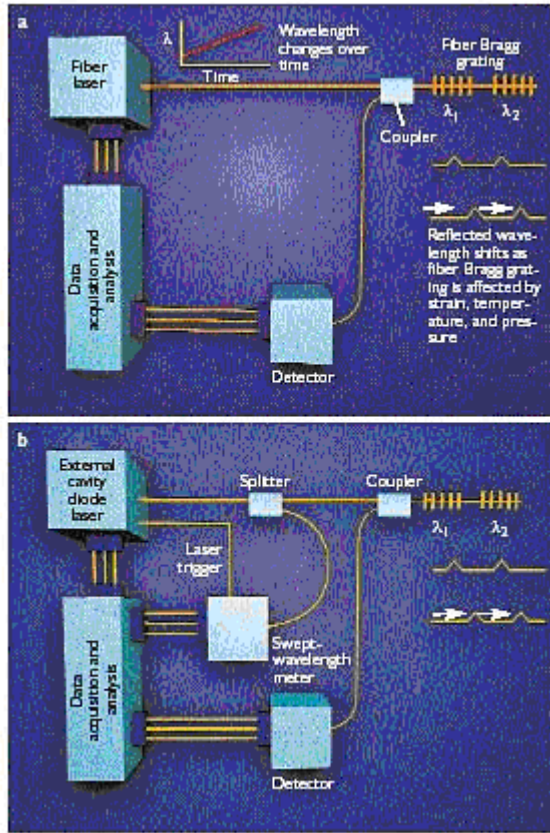


Figure 6: Two laser/detection systems that measure the wavelength shifts in fiber Bragg gratings resulting from strain, temperature, or acoustic changes.

have lower scan frequencies than those using fiber lasers, developments in ECDL technology will soon provide ultra fast tuning rates of up to 10,000 nm/s, enabling both high-speed and highly accurate sensing systems (Fig.6).

The *sensitivity* of a typical *FBG* sensor can be estimated by using the following relation between induced strain and voltage measured at the photodetector

$$\frac{dV}{d\epsilon} = \frac{dR}{d\epsilon} (Z_{PD} \times P_o)$$

where, V is voltage, P_o is the optical source power, ϵ is strain, R is the reflectivity of the grating at a specific wavelength and Θ is the photodiode

sensitivity (A/W) and Z_{PD} is the resistance of in the photodiode circuit. For typical values: $P_o = 1.5$ mW (50% of a 3mW laser is coupled into the fiber), *FBG* sensitivity ratio $dR/d\epsilon = 2.310^{-3}$ ($1/\mu\epsilon$), $Z_{PD} = 10M\Omega$, and a photo-detector sensitivity of $\Theta = 0.97$ A/W resulting in a *FBG* sensor sensitivity of

$$\frac{dV}{d\epsilon} = 30 \text{ V}/M\Omega$$

with a minimum detectable strain (dark current limited) of approximately, $0.001 \mu\epsilon$. For comparison, a high quality piezoelectric transducer has a sensitivity of approximately

$$\frac{dV}{d\epsilon} = 2600 \text{ V}/M\Omega$$

with a minimum detectable strain of approximately $3 \mu\epsilon$. The immediate result is that while the optical system has a significantly smaller voltage sensitivity per unit micro-strain, the noise floor has improved by several order of magnitude over the piezo-ceramic element. This estimate is based on a quasi steady state assumptions for a strain measurement. Extending this estimate to the MHz range for dynamic measurements is acceptable and has been verified by experimental measurements reported literature.^{29,30} The application for the proposed system measurements would be a dynamic in nature on the order of 500 Hz to 75 kHz.

There is a wealth of existing technologies that the photonic industries have developed for the telecommunications applications. Wave Division Multiplexing (WDM) components revolutionized the information superhighway by dramatically increasing bandwidth capacity, which led to next-generation networks and the maturation of the photonic industry (see Fig. 7). Because companies needed these network components in large volumes and at narrower channel spacing, testing and measuring these devices required ever-faster, lower-noise tunable lasers. ECDLs were developed that could tune continuously at speeds of up to 100 nm/s over a wavelength range of 1520 to 1620 nm and with side-mode suppression ratios as high as 70 dB, which resulted in extremely low-noise performance. Because the lasers operated 24 hours a day, 7 days a week on the manufacturing floor often overseas they had to be rugged, reliable, and stable and meet strict shock and humidity standards. The resulting technology can be leveraged into numerous multi

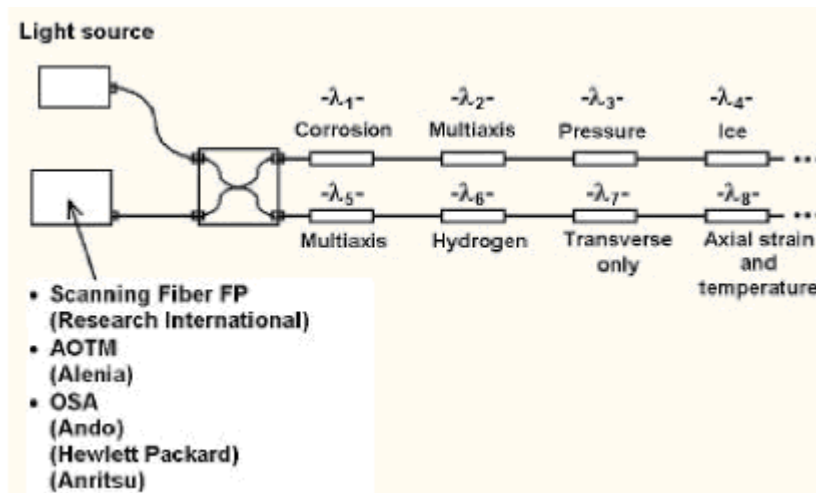


Figure 7: Multi-sensing *FBG* array.

sensor applications all along the length of a single fiber or group of fibers. The large selection of component manufactures provides a robust source of reliable components with long operational life times in excess of 100,000 hrs continuous use.³¹

This completes the description of the cylindrical shell process and measurement models used in these experiments, next we consider the development of a model-based detection scheme.

III. MODEL-BASED DETECTION

In this section we discuss the design of a detector to monitor the performance of the model-based processor and indicate when the model is no longer adequate or does not track the measured data. First, we briefly develop the required theory. Once this is accomplished, we then discuss the development of a practical processor and apply it to our simulated data sets.

Developing the model-based processor for the vibrational detection problem is based on a stochastic representation of the underlying dynamical state-space system of the previous section (see Eq. 3). We use a continuous-discrete Gauss-Markov representation, that is, excite the system with white Gaussian noise and take into account the measurement uncertainty

$$\begin{aligned}
\dot{x}(t) &= Ax(t) + Bu(t) + w(t) && \text{for } w \sim \mathcal{N}(0, R_{ww}) \\
y(t_k) &= Cx(t_k) + v(t_k) && \text{for } v \sim \mathcal{N}(0, R_{vv})
\end{aligned} \tag{5}$$

where t_k is the sample time at the output of the digitizer (analog-to-digital converter) and the initial state is assumed Gaussian, $x(0) \sim \mathcal{N}(x(0), P(0))$. Thus, this represents a stochastic extension of the deterministic system. The vibrational response as well as states are contaminated with noise and uncertainties (unknown parameters); therefore, we formulate the enhancement problem as a state/response estimation problem using an embedded model developed from first principles or “fit” to the data using parameter estimation techniques. In any case the vibrational system enhancement problem can be formulated succinctly as:

GIVEN a set of noisy response sampled-measurements, $\{y(t_k)\}$ and known excitations, $\{u(t)\}$ along with the corresponding Gauss-Markov model of Eq. 5, FIND the best estimate of the response (and state), $\hat{y}(t_k)$ ($\hat{x}(t_k|t_k)$).

The optimal solution to this problem is well-known⁸ and is given (succinctly) by:

$$\begin{aligned}
\hat{\dot{x}}(t_k|t_k) &= A\hat{x}(t_k|t_k) + K(t_k)\epsilon(t_k) \\
\epsilon(t_k) &= y(t_k) - \hat{y}(t_k) \\
\hat{y}(t_k) &= C\hat{x}(t_k|t_k)
\end{aligned} \tag{6}$$

Thus, based on the assumed Gauss-Markov model, the optimum processor or Kalman filter has the known excitation ($u(t)$) and noisy measurement data ($y(t_k)$) as input and produces an estimate of the states ($\hat{x}(t_k|t_k)$), filtered response measurement ($\hat{y}(t_k)$) and the residual or *innovations* sequence, ($\epsilon(t_k)$), as output. The statistical properties of the innovations are used to assess the performance of the processor, since a necessary and sufficient condition for the *MBP* to be optimal is that the innovations sequence *must* be *zero-mean* and *white*.⁸ The innovations sequence is zero-mean and white *only* when the process and measurement models reflect the true vibrational response (and states) for a properly tuned *MBP*. Statistical changes in $\epsilon(t_k)$, reflect changes from the normal or expected operation; therefore, we can utilize these changes to *monitor* the performance of the model embedded in the

processor. First, we develop the theoretical monitor. From the insight we gain in its development, we then investigate a more pragmatic approach and apply it to our vibrational problem.

Theoretically, it can be shown that when “model mismatch” occurs, the innovations become non-zero mean and are no longer white; therefore, we must develop a monitor to *decide* whether or not the innovations satisfy the required properties for optimality.^{8–11} Assuming a normal (no failures) structure initially, the *MBP* is tuned to produce a zero-mean, white innovations establishing the *normality* operating condition. When something changes in the structure due to excessive vibrations or aging failure, the underlying normal vibrational model will no longer “match” the measured response data indicating a change from normal condition to what we define as *abnormal* alerting us to a potential failure as described previously in Fig. 2; therefore, we declare a failure and attempt to classify its type. This is the basic principle^{8–11} of the vibrational failure monitor/detector or more properly “change detector.”

To formally pose this problem, we appeal to classical (sequential) detection theory.²⁰ We are to test the binary hypothesis that the innovations sequence is zero-mean and white

$$\begin{aligned} \mathcal{H}_0 : \quad \epsilon(t_k) &\sim \mathcal{N}(0, R_{\epsilon\epsilon}(t_k)) && \text{[WHITE]} \\ \mathcal{H}_1 : \quad \epsilon(t_k) &\sim \mathcal{N}(\bar{\mu}_\epsilon, \bar{R}_{\epsilon\epsilon}(t_k)) && \text{[NON-WHITE]} \end{aligned} \quad (7)$$

which is a statistical test for the zero-mean and whiteness of the innovations sequence. Note that we assume that we *know* the model error and how to calculate $\bar{\mu}_\epsilon(t_k)$ and $\bar{R}_{\epsilon\epsilon}(t_k)$ a-priori.

The optimal solution to this binary detection problem is based on applying the *Neyman-Pearson theorem* leading to the likelihood ratio²³ and is given by the ratio of probabilities for the *sequential innovations detector* (*SID*), that is,

$$\mathcal{L}[\mathcal{E}_{t_N}] := \frac{\Pr(\mathcal{E}_{t_N}|\mathcal{H}_1)}{\Pr(\mathcal{E}_{t_N}|\mathcal{H}_0)} \begin{array}{l} \mathcal{H}_1 \\ > \\ < \\ \mathcal{H}_0 \end{array} \tau \quad (8)$$

where $\mathcal{E}_{t_N} := \{\epsilon(t_0), \epsilon(t_1), \dots, \epsilon(t_N)\}$ or expanding

$$\mathcal{L}[\mathcal{E}_{t_N}] = \frac{\Pr(\epsilon(t_0), \epsilon(t_1), \dots, \epsilon(t_N) | \mathcal{H}_1)}{\Pr(\epsilon(t_0), \epsilon(t_1), \dots, \epsilon(t_N) | \mathcal{H}_0)} \quad (9)$$

but from the chain rule of probability⁸, we have that

$$\Pr(\mathcal{E}_{t_k} | \mathcal{H}_i) = \Pr(\epsilon(t_k) | \mathcal{E}_{t_{k-1}}; \mathcal{H}_i) \times \dots \times \Pr(\epsilon(t_1) | \epsilon(t_0); \mathcal{H}_i) \times \Pr(\epsilon(t_0) | \mathcal{H}_i) \quad (10)$$

which can be expressed succinctly using Bayes' rule as

$$\Pr(\mathcal{E}_{t_k} | \mathcal{H}_i) = \Pr(\epsilon(t_k), \mathcal{E}_{t_{k-1}} | \mathcal{H}_i) = \Pr(\epsilon(t_k) | \mathcal{E}_{t_{k-1}}; \mathcal{H}_i) \times \Pr(\mathcal{E}_{t_{k-1}} | \mathcal{H}_i) \quad (11)$$

Substituting these expressions (replacing t_N by t_k) into Eq. 8 and grouping we obtain

$$\mathcal{L}[\mathcal{E}_{t_k}] = \left[\frac{\Pr(\mathcal{E}_{t_{k-1}} | \mathcal{H}_1)}{\Pr(\mathcal{E}_{t_{k-1}} | \mathcal{H}_0)} \right] \times \frac{\Pr(\epsilon(t_k) | \mathcal{E}_{t_{k-1}}; \mathcal{H}_1)}{\Pr(\epsilon(t_k) | \mathcal{E}_{t_{k-1}}; \mathcal{H}_0)} \quad (12)$$

and therefore, we have the recursion or equivalently sequential likelihood as

$$\mathcal{L}[\mathcal{E}_{t_k}] := \mathcal{L}[\mathcal{E}_{t_{k-1}}] \frac{\Pr(\epsilon(t_k) | \mathcal{E}_{t_{k-1}}; \mathcal{H}_1)}{\Pr(\epsilon(t_k) | \mathcal{E}_{t_{k-1}}; \mathcal{H}_0)} \quad (13)$$

Taking logarithms we obtain the relation for the *sequential log-likelihood*

$$\lambda_\epsilon(t_k) := \ln \mathcal{L}[\mathcal{E}_{t_k}] = \lambda_\epsilon(t_{k-1}) + \ln \Pr(\epsilon(t_k) | \mathcal{E}_{t_{k-1}}, \mathcal{H}_1) - \ln \Pr(\epsilon(t_k) | \mathcal{E}_{t_{k-1}}, \mathcal{H}_0) \quad (14)$$

The corresponding Wald or *sequential probability ratio test*⁸ is then given by:

$$\begin{aligned} \lambda_\epsilon(t_k) &\geq \tau_1 && \text{Accept } \mathcal{H}_1 \\ \tau_0 &\leq \lambda_\epsilon(t_k) \leq \tau_1 && \text{Continue} \\ \lambda_\epsilon(t_k) &\leq \tau_0 && \text{Accept } \mathcal{H}_0 \end{aligned} \quad (15)$$

and the underlying conditional Gaussian distributions are given by

$$\Pr(\epsilon(t_k) | \mathcal{E}_{t_{k-1}}, \mathcal{H}_0) = (2\pi)^{-N/2} |\mathbf{R}_{cc}(t_k)|^{-1/2} \exp\left(-\frac{1}{2} \epsilon'(t_k) \mathbf{R}_{cc}^{-1}(t_k) \epsilon(t_k)\right) \quad (16)$$

and

$$\Pr(\epsilon(t_k) | \mathcal{E}_{t_{k-1}}, \mathcal{H}_1) = (2\pi)^{-N/2} |\bar{\mathbf{R}}_{\epsilon\epsilon}(t_k)|^{-1/2} \exp\left(-\frac{1}{2}(\epsilon(t_k) - \bar{\mu}_\epsilon(t_k))' \bar{\mathbf{R}}_{\epsilon\epsilon}^{-1}(t_k) (\epsilon(t_k) - \bar{\mu}_\epsilon(t_k))\right) \quad (17)$$

If we include the determinants in the thresholds, we have the modified decision function

$$\Lambda_\epsilon(t_k) = \Lambda_\epsilon(t_{k-1}) + \frac{1}{2} \epsilon'(t_k) \mathbf{R}_{\epsilon\epsilon}^{-1}(t_k) \epsilon(t_k) - \frac{1}{2} (\epsilon(t_k) - \bar{\mu}_\epsilon(t_k))' \bar{\mathbf{R}}_{\epsilon\epsilon}^{-1}(t_k) (\epsilon(t_k) - \bar{\mu}_\epsilon(t_k)) \quad (18)$$

which yields the new test

$$\begin{aligned} \Lambda_\epsilon(t_k) &\geq \Upsilon_1 && \text{Accept } \mathcal{H}_1 \\ \Upsilon_0 &\leq \Lambda_\epsilon(t_k) \leq \Upsilon_1 && \text{Continue} \\ \Lambda_\epsilon(t_k) &\leq \Upsilon_0 && \text{Accept } \mathcal{H}_0 \end{aligned} \quad (19)$$

where

$$\begin{aligned} \Upsilon_1 &= \tau_1 + \frac{1}{2} \ln |\mathbf{R}_{\epsilon\epsilon}(t_k)|^{-1/2} - \frac{1}{2} |\bar{\mathbf{R}}_{\epsilon\epsilon}(t_k)|^{-1/2} \\ \Upsilon_0 &= \tau_0 + \frac{1}{2} \ln |\mathbf{R}_{\epsilon\epsilon}(t_k)|^{-1/2} - \frac{1}{2} |\bar{\mathbf{R}}_{\epsilon\epsilon}(t_k)|^{-1/2} \end{aligned} \quad (20)$$

The implementation of this monitor presents some basic problems, such as how to obtain estimates of the innovations (abnormal) mean and covariance required, but does illustrate a potential optimal solution to the model monitoring problem. As mentioned, the SID requires a-priori knowledge of the actual model “mismatch” and structurally how it enters the process model to obtain $[\bar{\mu}_\epsilon(t_k), \bar{\mathbf{R}}_{\epsilon\epsilon}(t_k)]$ for the monitor.^{16–18} In some cases, if the innovations are assumed ergodic, then a composite hypothesis test can be constructed using sample statistical estimators for the required statistics.⁸ When the processor is “tuned”, it provides an optimal or minimum (error) variance estimate of the state. The innovations sequence, which was instrumental in deriving the processor, also provides the starting point to check the *MBP* operation. Recall that a *necessary and sufficient condition* for a *MBP* to be optimal is that the innovation sequence is zero-mean and white. These are the first properties that must be evaluated to insure that the processor is

operating properly. If we assume that the innovation sequence is ergodic and Gaussian, then we can use the sample mean as the test statistic to estimate μ_ϵ , the population mean.⁸ The sample mean for the i^{th} component of ϵ_i is given by

$$\hat{\mu}_\epsilon(i) = \frac{1}{N} \sum_{t=1}^N \epsilon_i(t_k) \quad \text{for } i = 1, \dots, N_y \quad (21)$$

where $\hat{\mu}_\epsilon(i) \sim \mathcal{N}(\mu_\epsilon, R_{\epsilon\epsilon}(i)/N)$ and N is the number of data samples. We perform a statistical hypothesis test to “decide” if the innovation mean is null.⁸ We test that the mean of the i^{th} component of the innovation vector $\epsilon_i(t_k)$ is

$$\begin{aligned} \mathcal{H}_0 : & \quad \mu_\epsilon(i) = 0 \\ \mathcal{H}_1 : & \quad \mu_\epsilon(i) \neq 0 \end{aligned}$$

As our test statistic we use the sample mean. At the α -significance level, the probability of rejecting the null hypothesis \mathcal{H}_0 is given by

$$\Pr \left(\left| \frac{\hat{\mu}_\epsilon(i) - \mu_\epsilon(i)}{\sqrt{R_{\epsilon\epsilon}(i)/N}} > \frac{\tau_i - \mu_\epsilon(i)}{\sqrt{R_{\epsilon\epsilon}(i)/N}} \right| \right) = \alpha \quad (22)$$

Therefore, the *zero-mean test*,⁸ on each component innovation ϵ_i is given by

$$\begin{aligned} & > \text{Reject } \mathcal{H}_0 \\ \hat{\mu}_\epsilon(t_k) & & \tau_i \\ & < \text{Accept } \mathcal{H}_0 \end{aligned} \quad (23)$$

Under the null hypothesis \mathcal{H}_0 , each $\mu_\epsilon(i)$ is assumed zero. Therefore, at the 5 % significance level ($\alpha = 0.05$), we have that the threshold is

$$\tau_i = 1.96 \sqrt{\frac{\hat{R}_{\epsilon\epsilon}(i)}{N}} \quad (24)$$

where $\hat{R}_{\epsilon\epsilon}(i)$ is the *sample variance* (assuming ergodicity) estimated by

$$\hat{R}_{\epsilon\epsilon}(i) = \frac{1}{N} \sum_{t=1}^N \epsilon_i^2(t_k) \quad (25)$$

Under the same assumptions, we can perform a *whiteness test*,⁸ that is, check statistically that the innovations covariance corresponds to that of an uncorrelated (white) sequence. Assuming ergodicity of the innovations sequence, we use the sample covariance function as our test statistic with the i^{th} component covariance and lag k given by

$$\hat{R}_{\epsilon\epsilon}(i, k) = \frac{1}{N} \sum_{t=k+1}^N (\epsilon_i(t_k) - \hat{\mu}_\epsilon(i)) (\epsilon_i(t_k + k) - \hat{\mu}_\epsilon(i)) \quad (26)$$

We actually use the *normalized covariance* test statistic

$$\hat{\rho}_{\epsilon\epsilon}(i, k) = \frac{\hat{R}_{\epsilon\epsilon}(i, k)}{\hat{R}_{\epsilon\epsilon}(i)} \quad (27)$$

Asymptotically for large N , it can be shown that (see Refr. ¹¹) that

$$\hat{\rho}_{\epsilon\epsilon}(i, k) \sim \mathcal{N}(0, 1/N)$$

Therefore, the 95% confidence interval estimate is

$$I_{\rho_{\epsilon\epsilon}} = \hat{\rho}_{\epsilon\epsilon}(i, k) \pm \frac{1.96}{\sqrt{N}} \quad \text{for } N > 30 \quad (28)$$

Hence, under the null hypothesis, 95% of the $\hat{\rho}_{\epsilon\epsilon}(i, k)$ values must lie within this confidence interval to accept \mathcal{H}_0 . That is, for each *component* innovation sequence to be considered statistically white. The *whiteness test* of Eq. 28 is very useful to detect modeling inaccuracies from individual component innovations. However, for complex systems with a large number of measurement channels, it becomes computationally burdensome to investigate each innovation component-wise especially under the limiting ergodicity assumptions.

A statistic containing *all* of the innovation information is the *weighted sum-squared residual (WSSR)*. It aggregates all of the innovation *vector* information over some finite window of length M . It can be shown that the *WSSR* is related to a maximum-likelihood estimate of the normalized innovations variance.^{10,11} The *WSSR* test statistic is given by

$$\rho_\epsilon(\ell) := \sum_{k=\ell-M+1}^{\ell} \epsilon'(k) R_{\epsilon\epsilon}^{-1}(k) \epsilon(k) \quad \text{for } \ell \geq M \quad \epsilon \in \mathcal{R}^{N_\epsilon \times 1} \quad (29)$$

The *WSSR* hypothesis test is based on

$$\mathcal{H}_0 : \quad \rho_\epsilon(\ell) \text{ [WHITE]}$$

$$\mathcal{H}_1 : \quad \rho_\epsilon(\ell) \text{ [NON-WHITE]}$$

and is given by

$$\rho_\epsilon(\ell) \begin{matrix} > & \tau_1 \\ & \tau \\ < & \tau_0 \end{matrix} \quad (30)$$

Under the null hypothesis, the *WSSR* is chi-squared distributed, $\rho_\epsilon(\ell) \sim \chi^2(N_\epsilon M)$. However, for $N_\epsilon M > 30$, $\rho(\ell)$ is approximately Gaussian $\mathcal{N}(N_\epsilon M, 2N_\epsilon M)$ (see ⁸⁻¹¹ for more details). At the α -significance level, the probability of rejecting the null hypothesis is given by

$$Pr \left(\left| \frac{\rho(\ell) - N_\epsilon M}{\sqrt{2N_\epsilon M}} > \frac{\tau - N_\epsilon M}{\sqrt{2N_\epsilon M}} \right| \right) = \alpha \quad (31)$$

For a level of significance of $\alpha = 0.05$, we have

$$\tau = N_\epsilon M + 1.96\sqrt{2N_\epsilon M} \quad (32)$$

Thus, we see that the *WSSR* can be considered a “whiteness test” of the innovations *vector* over a finite window of length N . Note that since $[\{\epsilon(t_k)\}, \{R_{\epsilon\epsilon}(t_k)\}]$ are obtained from the state-space *MBP* algorithm directly, they can be used for both *stationary* as well as *nonstationary* processes. In fact, in practice for a large number of measurement components, the *WSSR* is used to “tune” the filter and then the component innovations are individually extracted and checked for zero-mean/whiteness to detect failures. Note also that the adjustable parameter of the *WSSR* statistic is the window length M , which essentially controls the width of the window sliding through the

innovations sequence. Therefore, even if we cannot implement the optimal *SID*, we can still perform a set of pragmatic statistical hypothesis tests to investigate the condition of the underlying structure and classify its failure.

IV. FAILURE DETECTION AND CLASSIFICATION

In this section we extend the basic principles of model-based detection and apply them to our particular problem of cylindrical failure monitoring and classification. First we start with the development of a “normal” model ($\Sigma_{\mathcal{N}}$) providing a standard for monitoring and comparison. Here we assume that we have measured the vibrational response of the structural system (cylinder in our case) and developed a *model* to capture its performance, that is, the normal (state-space) system, $\Sigma_{\mathcal{N}} := \{A_{\mathcal{N}}, B_{\mathcal{N}}, C_{\mathcal{N}}\}$ is characterized by the structural matrices of Eq. 3. We measure an ensemble of vibrational responses from the system using a controlled excitation over the frequency range of interest and then use them to obtain a representative model by averaging over the estimated parameters for each realization, $y_{\ell}(t_k)$; $\ell = 1, \dots, L$. That is, we “fit” a model to the ℓ^{th} realization

$$\Sigma_{\mathcal{N}}(\Theta_{\ell}) := \{A_{\mathcal{N}}(\Theta_{\ell}), B_{\mathcal{N}}(\Theta_{\ell}), C_{\mathcal{N}}(\Theta_{\ell})\} \quad (33)$$

and then average over the entire ensemble

$$\bar{\Sigma}_{\mathcal{N}}(\Theta) := E_{\Theta}\{\Sigma_{\mathcal{N}}(\Theta_{\ell})\} = \sum_{\ell=1}^L \bar{\Sigma}_{\mathcal{N}}(\Theta_{\ell}) = \{\bar{A}_{\mathcal{N}}(\Theta), \bar{B}_{\mathcal{N}}(\Theta), \bar{C}_{\mathcal{N}}(\Theta)\} \quad (34)$$

A model order (dimension of the $A_{\mathcal{N}}$) is selected to guarantee a zero-mean/white innovations sequence using the ensemble as

$$\epsilon(t_k; \Theta_{\ell}) = y_{\ell}(t_k) - \hat{y}(t_k; \Theta_{\ell}) \quad \text{for } \ell = 1, \dots, L \quad (35)$$

The model extraction (parameter estimation) and validation method is shown in Fig. 8. Here we see that an initial normal model is estimated from part of the ensemble data (training data) to generate a set of parameters producing an average model (above). Next the parameterized model is applied to test data where the innovations sequence is generated and tested for acceptability. If acceptable, the parameter ($\Theta_{\mathcal{N}}$) is adjusted (averaged)

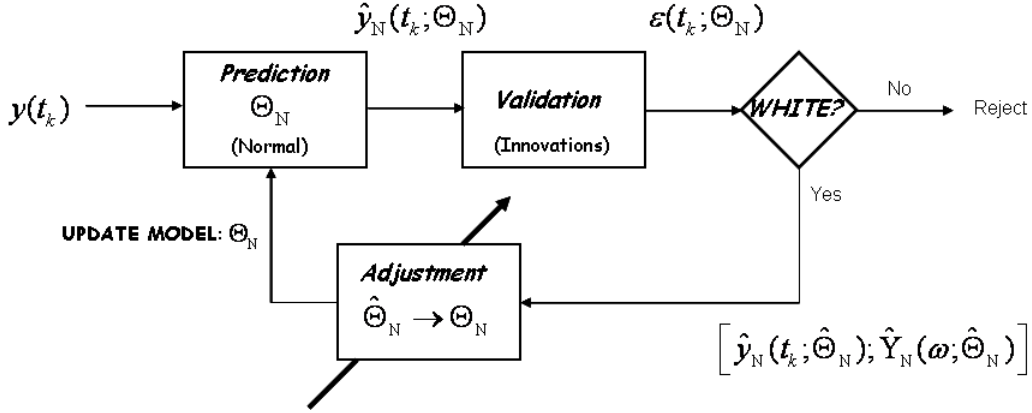


Figure 8: Normal vibrational model extraction and validation: Ensemble parameter estimation/prediction, prediction error whiteness, model parameter updating.

and the model is updated yielding an acceptable system model. In this way the *normal model* is trained, tested and validated over an ensemble of both training and test data to ensure its validity.

Once we have performed the parameter estimation,⁸ we construct the state-space model from its parameters. Since we use a prediction error parameter estimation technique, the resulting state-space model is the discrete (sampled) *innovations model* parameterized by the following:

$$\begin{aligned}
 \hat{x}(t_k|t_k) &= A(\Theta_{\mathcal{N}})\hat{x}(t_k|t_{k-1}) + K(t_k; \Theta_{\mathcal{N}})\epsilon(t_k; \Theta_{\mathcal{N}}) \\
 \epsilon(t_k; \Theta_{\mathcal{N}}) &= y(t_k) - \hat{y}(t_k; \Theta_{\mathcal{N}}) \\
 \hat{y}(t_k) &= C(\Theta_{\mathcal{N}})\hat{x}(t_k|t_{k-1})
 \end{aligned} \tag{36}$$

In our case, since we have two sensors available and we choose two positions to locate them (see Fig. 7c), then our vector measurement is given by $y(t_k; \mathbf{r})$ where \mathbf{r} is the sensor position vector on the structure. We will (tacitly) assume that the positions are weakly coupled at first and ignore the cross-coupling terms simplifying the models and measurements. Therefore, we separate the analysis of each subsystem defined by: $A(\Theta) = \text{diag}[A_1(\Theta) \ A_2(\Theta)]$. The subsystem model parameters will be “fit” to each subsystem individually and the measurements and detections processed ac-

cordingly. With this in mind we proceed to process the measured vibrational response data from the cylinder.

A. Cylinder Vibrational Response Normal Model

The normal model is developed using the parameter estimation techniques resulting in the innovations model of Eq. 36. A typical set of cylindric response data is shown in Fig. 9 where we see the noisy time series measurements and corresponding power spectra. The cylinder excitation was a chirp (swept sinusoid) that was varied from $100Hz$ to $5kHz$. This range was selected from numerical model studies^{5,6} of the cylinder. Next the models were fit as discussed above with the validation over a test ensemble (30 members) of vibrational response measurements. A typical fit and validation are shown in Fig. 10 where we observe the innovations sequence in (a) with the associated zero-mean/whiteness and $WSSR$ statistic in (b) and (c). This realization passes the “whiteness” criteria tests and is acceptable for model updating (averaging) parameters.

With the average normal (pristine) model validated in terms of the ensemble zero-mean/whiteness testing, a set of data were generated to test the performance of the estimated prediction model. The results for this tests are shown in Fig. 11. In *a*, we see the results for both sensors. Here we observe that from an ensemble of 30 ($\times 2$ sensors) that 100% of the innovations (correlation) lie within 10% out while 75% were “statically white” lying within the 5% out bounds for sensor 1. The sensor 2 results were above the 5% bound with 93% of the ensemble below the 10% bound. These results indicate that the estimated average prediction model (Fig. 8) is adequate for failure detection processing. Next we create failure conditions by attaching masses at the end of the cylinder: one of 300gm and one of 150gm. The resulting spectra for both sensors are shown in Fig. 12 where we also indicate the number of resonant peaks residing in the 1000-2000 Hz band. We note that for sensor 1 the number of resonant peaks under normal conditions are 5, while for the 150gm and 300gm masses the number increases to (10,10) and (12,8), respectively. Thus, we expect a more challenging detection problem when using sensor 2 responses. In conclusion, we see that both models from the sensor positions are obtained and indicate a robust model able to pass the ensemble data demonstrating the robustness of the models.

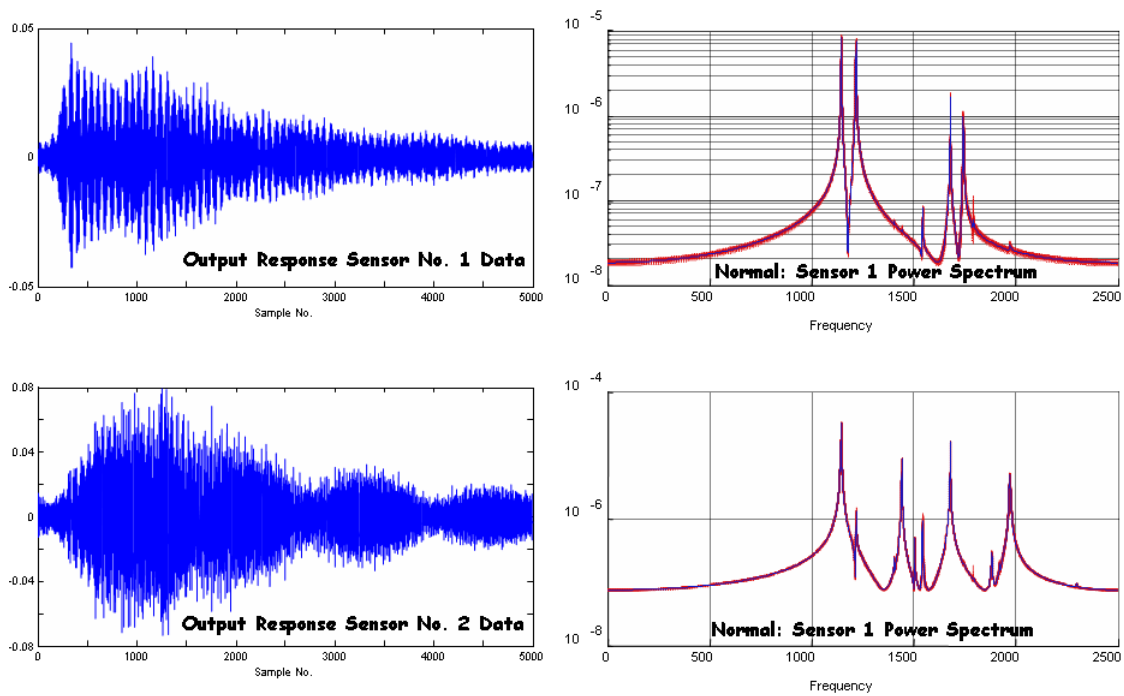


Figure 9: Cylinder vibrational response data: Time series and power spectra for each sensor with the number of resonant peaks (5,8) for sensors 1 and 2, respectively.

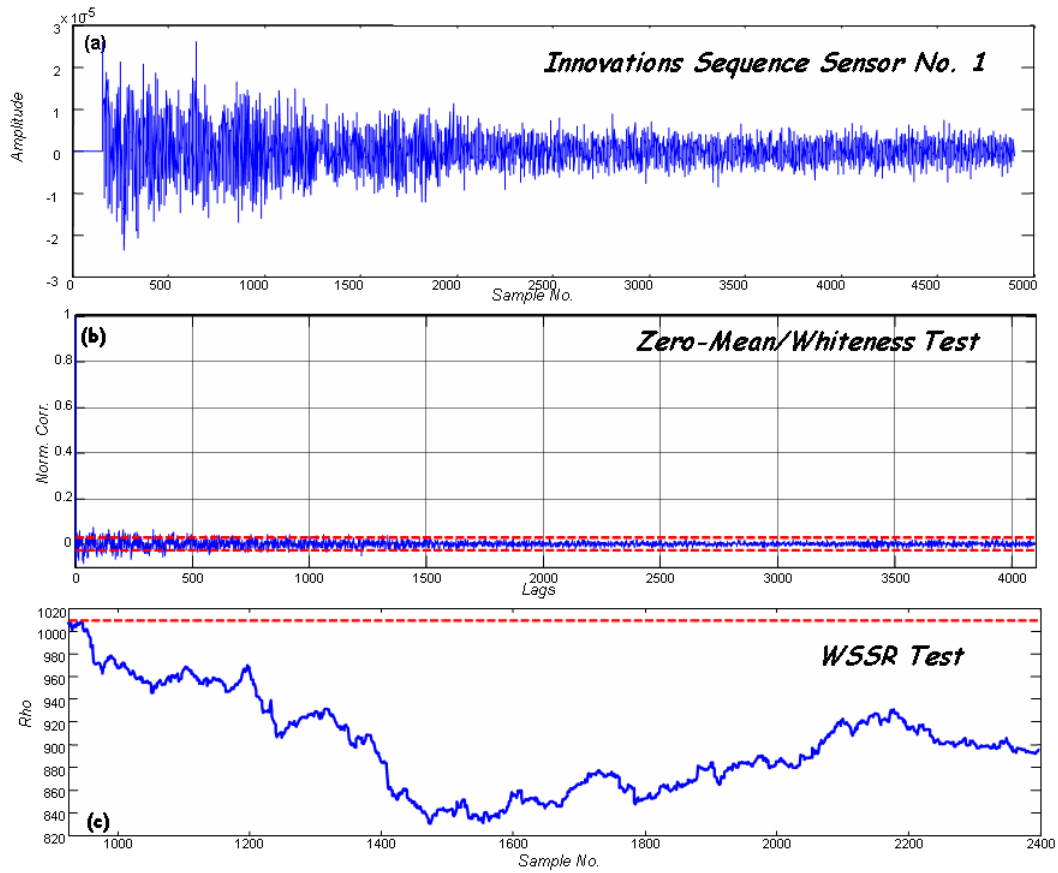


Figure 10: Ensemble zero-mean/whiteness and validation testing for normal cylinder vibrational models. (a) Innovations sequence. (b) Zero-Mean/Whiteness Test. (c) WSSR test.

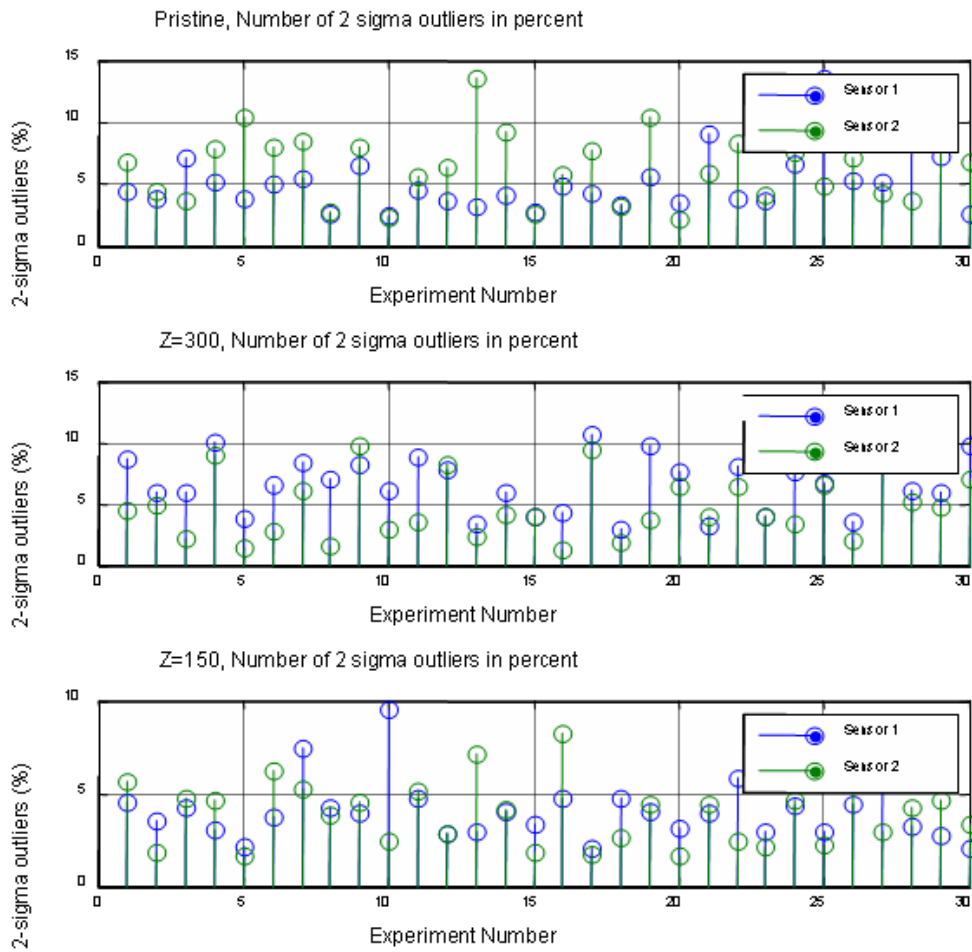


Figure 11: Self-validation ensemble whiteness test results for vibrational models: (a) Normal (pristine) model self-validation. (b) Failure model for 300 gm mass self-validation. (c) Failure model for 150 gm mass self-validation.

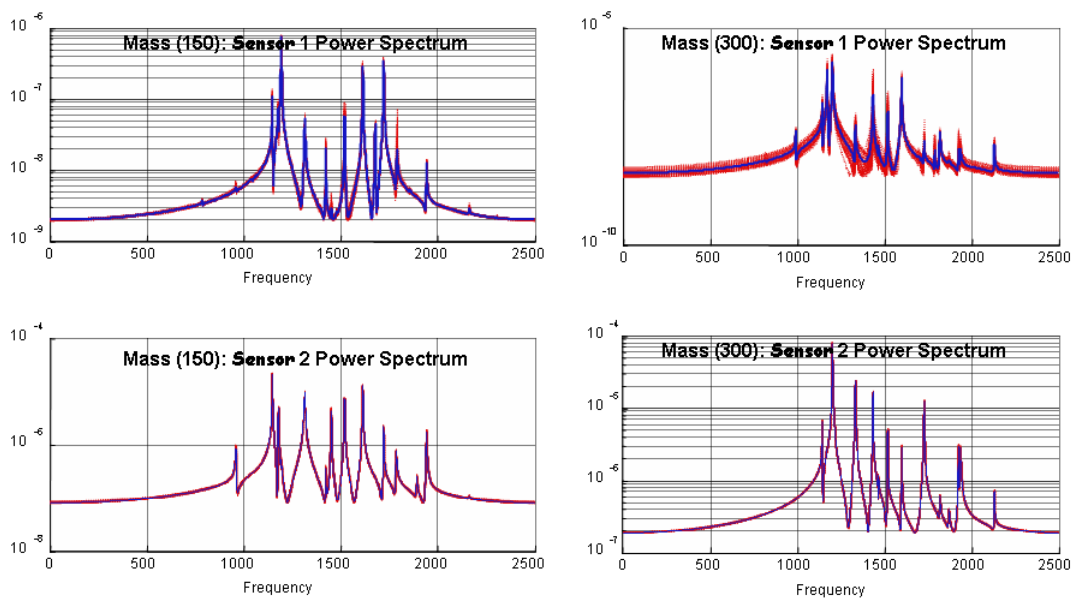


Figure 12: Sensor spectra for failure conditions: (a) 150 gm mass spectra from sensor 1 (10 resonant peaks). (b) 150 gm mass spectra from sensor 2 (10 resonant peaks). (c) 300 gm mass spectra from sensor 1 (12 resonant peaks). (d) 300 gm mass spectra from sensor 2 (8 resonant peaks).

IV. RESULTS

Failure conditions were created by attaching the specified mass for each experiment and generating a corresponding ensemble (30 members) of resonance data for performance testing. The failure detections using the average normal (pristine) model was applied after validation tests (above) were performed indicating the robustness of the embedded processor model. The results are shown in Fig. 13 for both sensors and both cases (150 gm/300 gm). From the figure we see that the failure detector performs quite well. For the 300gm mass induced failure conditions all of the members of the test ensemble were *detected* successfully with over $> 60\%$ bound (non-white), that is, recall to be declared normal each test should lie within the 5% whiteness bound—these failures exceed $> 60\%$ for sensor 1 and $> 55\%$ for sensor 2. The results for the 150gm mass induced failure conditions are slightly better with failures exceeding $> 60\%$ in each run for sensor 1 and $> 58\%$ for sensor 2.

Failure classification (fig. 2) is performed in a similar manner. Once the failure is detected, the corresponding *abnormal* (failure) model is now developed following the same techniques as for the *normal* model development. The abnormal models are estimated and validated as shown in Fig. 7b,c and then used to process the “failure” data to classify each individual mechanism. The validation runs indicate the robustness of these models using a failure classifier constructed identically to that of Fig. 8. This model-based⁸ approach appears to perform quite well for both detection and classification.

As a final part of the analysis we estimate the residual sequence comparing the normal spectra to that of the failure (induced) spectra and the results are shown in Fig. 14. Clearly there are spectral differences induced by the attached mass as illustrated by the figure. The differences are quite interesting for this particular location of the mass, sensor 1 shows a large spectral difference from the normal compared to that of sensor 2 indicating that is more sensitive to this vibrational response.

This completes the discussion of the results, next we conclude and discuss future effort.

V. CONCLUSIONS

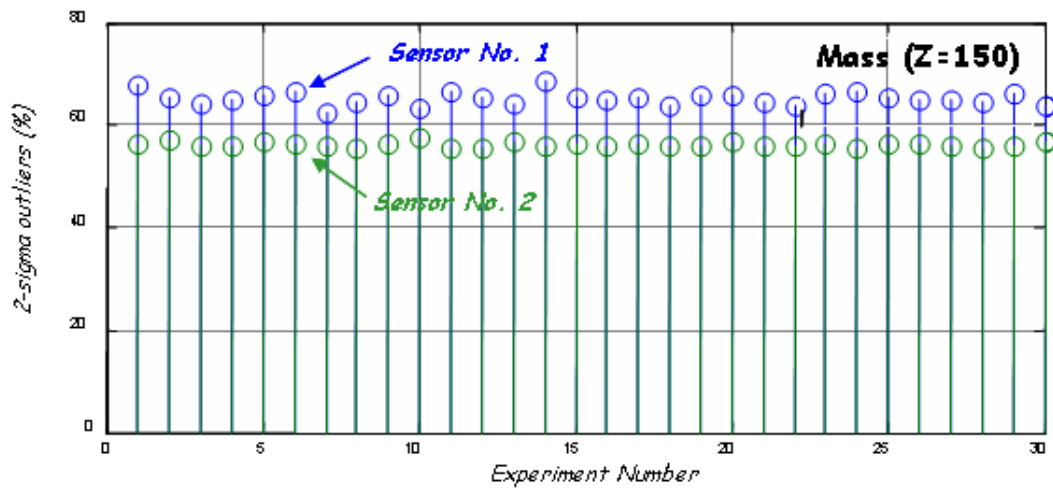
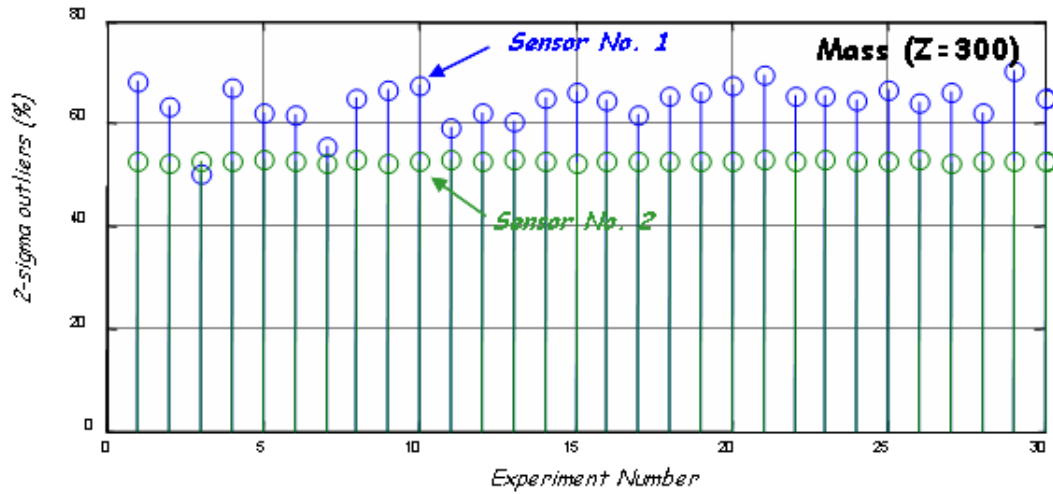


Figure 13: Failure detector performance on vibrational test data: (a) 300gm mass induced failure condition for sensors 1 and 2 (> 60% out, > 55% out). (b) 150gm mass induced failure condition for sensors 1 and 2 (> 60% out, > 58% out).

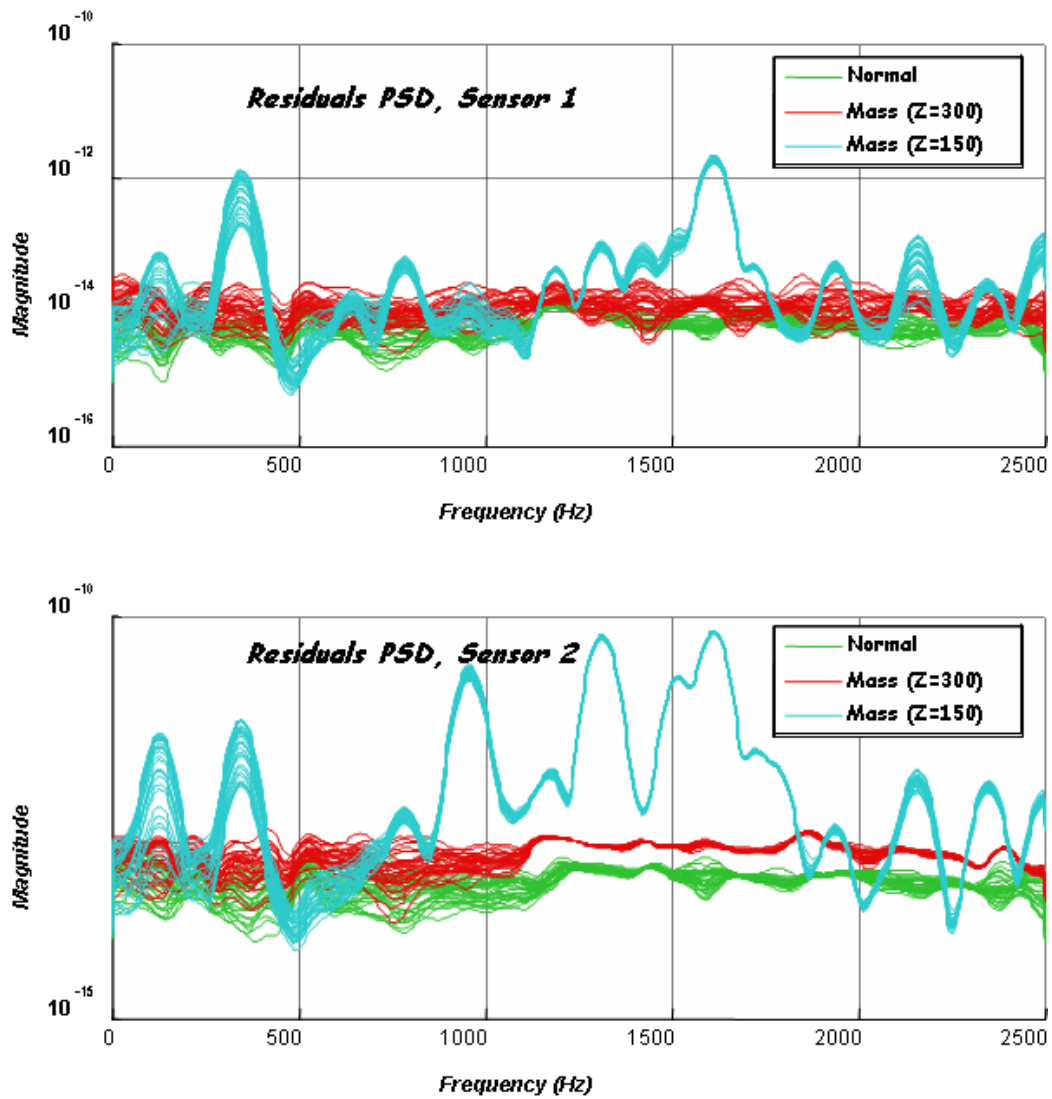


Figure 14: Estimated spectral residuals with normal spectrum: (a) Mass induced failure condition for sensor 1. (b) Mass induced failure condition for sensor 2.

We have demonstrated the effectiveness of a model-based approach to failure detection and classification by performing parameter estimation and model-based detection on sets of vibrational response experimental data. By investigating the response of data and fitting parametric models we were able to use whiteness testing of the innovations sequence to both validate and detect two sets of failure conditions induced by attaching masses to a cylindrical test object. The processor initially detects a departure from the *normal* structural condition indicating a failure and then proceeds to classify the particular failure mechanism by comparing to failure models developed in an identical manner. The results appear to indicate that this approach is viable.

Future efforts will be aimed at locating the failure itself by utilizing the residuals that can be extracted from the normal spectra when compared to the abnormal. Here the residual sequence is obtained again using the model-based approach as shown in Fig. 15.⁸ The required spectra are estimated using the average normal model ($\hat{Y}_{\text{mathcal{N}}}(\omega; \Theta)$) and the current failure model, ($\hat{Y}_{\text{mathcal{F}}}(\omega; \Theta)$) used to create the residual spectrum

$$R(\omega) = \hat{Y}_{\text{mathcal{N}}}(\omega; \Theta) - \hat{Y}_{\text{mathcal{F}}}(\omega; \Theta)$$

This spectrum is then backpropagated using a propagation model and like time-reversal focuses back on the failure position performing the desired localization. Preliminary results appear to be quite promising.

ACKNOWLEDGEMENTS

This work performed under the auspices of the U.S. Department of Energy by Lawrence Livermore National Laboratory under Contract DE-AC52-07NA27344.

¹ V. Wowk *Machinery Vibration: Measurement and Analysis*, (McGraw-Hill, New York, NY, 1991).

² H. C. Pusey and S. C. Pusey, *Focus on Mechanical Failures: Mechanisms and Detection*, (Vibration Institute, Willowbrook, IL, 1991).

³ A. D. Dimarogonas and S. Haddad, *Vibration for Engineers*, (Prentice-Hall, Englewood Cliffs, NJ, 1992).

⁴ C. J. Li, T. Kim, and G. W. Nickerson, "Screw compressor fault detection and diagnosis based on modeling and estimation," Proc. 45th Meeting

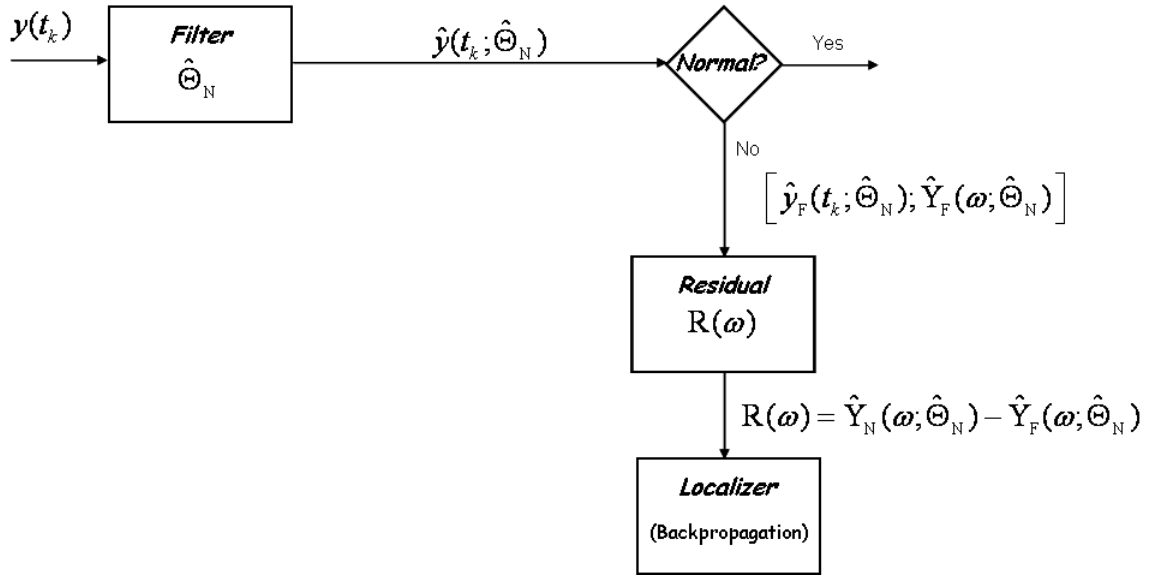


Figure 15: Failure localization using a propagation model and residual back-propagation after failure detection.

Mech. Failures Prevention Group, Annapolis, MD, pp. 35-45, 1991.

⁵ J. D. Achenbach, *Wave Propagation in Elastic Solids*, (Elsevier North-Holland, New York, NY, 1980).

⁶ O. C. Zienkiewicz, *The Finite Element Method*, (McGraw-Hill, New York, NY, 1983).

⁷ M. Basseville and I. Nikiforov, *Detection of Abrupt Changes: Theory and Application*, (Prentice-Hall, Englewood Cliffs, NJ, 1993).

⁸ J. V. Candy, *Model-Based Signal Processing*, (John Wiley/IEEE Press, Hoboken, NJ, 2006).

⁹ F. Gustafsson, *Adaptive Filtering and Change Detection*, (John Wiley/IEEE Press, Hoboken, NJ, 2000).

¹⁰ A. Willsky, "A survey of design methods for failure detection in dynamic systems," *Automatica*, Vol. **12**, pp. 601-611, (1976).

¹¹ R. Mehra and J. Peshon, "An innovations approach to fault detection and diagnosis in dynamical systems," *Automatica*, Vol. **7**, pp. 637-640, (1971).

¹² S. G. Azevedo, J. V. Candy and D. L. Lager, "On-line failure detection of vibrating structures," *Proc. ASME Conf. on Mechanical Vibrations and Noise*, Hartford, CT, (1980).

¹³ D. L. Lager, S. G. Azevedo, and J. V. Candy, "The application of large-scale state estimation to vibrating structures," Proc. 6th IFAC Symp. Identification System Param. Est., Wash., DC, (1983).

¹⁴ J. V. Candy and H. E. Jones, "Processing of prosthetic heart valve sounds for single leg separation classification," J. Acoust. Soc. Am., **97**, pp. 3663-3673, (1995).

¹⁵ J. V. Candy and H. E. Jones, "Classification of prosthetic heart valve sounds: a parametric approach," J. Acoust. Soc. Am., **97**, pp. 3675-3687, (1995).

¹⁶ J. V. Candy and R. B. Rozsa, "Safeguards design for a plutonium concentrator - an applied estimation approach," Automatica, Vol. 16, pp. 615-627 (1980).

¹⁷ J. V. Candy and E. J. Sullivan, "Ocean acoustic signal processing: a model-based approach," J. Acoust. Soc. Am., **92**, No. 6, pp. 3185-3201, (1992).

¹⁸ J. R. Roman and D. W. Davis, "State-space models for multichannel detection," Final Report for Contract No. F30602-92-C-0081, RL-TR-93-146, Rome Laboratory, Griffiss AFB, NY, (1993).

¹⁹ R. Luppold, J. R. Roman, and S. Roth, "Sensor diagnostics using the detection filter algorithm," Proc. 6th Digital Avionics Systems Conf., Baltimore, Md., (1984).

²⁰ A. Jazwinski, *Stochastic Processes and Filtering Theory*. (Academic Press, New York, NY, 1970).

²¹ L. Ljung, *System Identification: Theory for the User*. (Prentice-Hall, Englewood Cliffs, NJ, 1987).

²² P. Maybeck, *Stochastic Models, Estimation, and Control*. (Academic Press, New York, NY, 1979).

²³ H. Van Trees, *Detection, Estimation and Modulation Theory, Pt. 1*, (John Wiley, New York, NY, 1968).

²⁴ D. G. Childers, D. P. Skinner, and R. C. Kemerait, "The cepstrum: a guide to processing," Proc. IEEE, Vol. 65, No. 10, pp. 1428-1443, (1981).

²⁵ R. O. Duda and P. E. Hart, *Pattern Classification and Scene Analysis*, (John Wiley, New York, NY, 2001).

²⁶ D. F. Specht, "Probabilistic Neural Networks," Vol 3, Neural Networks, (1990).

²⁷ J. Beck and S-K. Au, "Bayesian updating of structural model and reliability using Markov Chain Monte Carlo simulation," J. Engr. Mech., Vol. **128**, No. 4, pp. 380-391, (2002).

²⁸ M. Wippich and K. Dessau, "Tunable lasers and fiber-bragg-grating sensors," *Web, AIP., The Industrial Physicist*, <http://www.aip.org/tip/INPHFA/vol-9/iss-3/p24.html>, (2003).

²⁹D. Betz, B. Thursby and W. Staszewski, "Acousto-ultrasonic sensing using fiber Bragg gratings," *Smart mater. Struct.* Vol. 12 pp. 122-128, (2003).

³⁰ P. Formitchov, S. Krishnaswamy, "Response of a fiber Bragg grating sensor," *Opt Eng.* Vol. 42(4), 9pp. 56-963, (2003).

³¹ E. Udd, W. Shultz, J. Seim, M. Morrell, T. Weaver, J. Bush, and G. Adamovsky, "Fiber optic distributed sensing systems for harsh aerospace environments." *SPIE*, Vol. 3674, pp. 136-144 (1999).